Journal of Applied Physics

Influence of variable Ca-doping on the critical current density of low-angle grain boundaries in $YBa_2Cu_3O_{7-d}$

Cite as: J. Appl. Phys. **128**, 103905 (2020); https://doi.org/10.1063/5.0016157
Submitted: 08 June 2020 . Accepted: 16 August 2020 . Published Online: 14 September 2020

Sang-il Kim, and David C. Larbalestier

View Online Export Citation CrossMark

ARTICLES YOU MAY BE INTERESTED IN

Rethinking the magnetic properties of lepidocrocite: A density functional theory and cluster expansion study
Journal of Applied Physics **128**, 103906 (2020); https://doi.org/10.1063/5.0009300

Point defects in two-dimensional hexagonal boron nitride: A perspective
Journal of Applied Physics **128**, 100902 (2020); https://doi.org/10.1063/5.0021093

Impact of dopant-induced optoelectronic tails on open-circuit voltage in arsenic-doped Cd(Se)Te solar cells
Journal of Applied Physics **128**, 103105 (2020); https://doi.org/10.1063/5.0018955

Challenge us.
What are your needs for periodic signal detection?
Watch

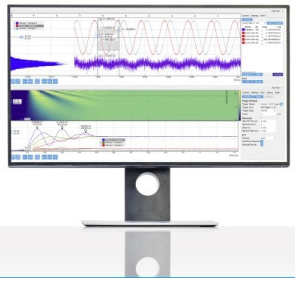

Zurich Instruments

© 2020 Author(s).

Journal of Applied Physics ARTICLE scitation.org/journal/jap

Influence of variable Ca-doping on the critical current density of low-angle grain boundaries in $YBa_2Cu_3O_{7-d}$

Cite as: J. Appl. Phys. **128**, 103905 (2020); doi: 10.1063/5.0016157
Submitted: 8 June 2020 · Accepted: 16 August 2020 ·
Published Online: 14 September 2020

View Online Export Citation CrossMark

Sang-il Kim[1] and David C. Larbalestier[2,a)]

AFFILIATIONS

[1]Department of Materials Science and Engineering, University of Seoul, Seoul 02504, South Korea
[2]National High Magnetic Field Laboratory, Florida State University, Tallahassee, Florida 32310, USA

[a)]**Author to whom correspondence should be addressed:** larbalestier@asc.magnet.fsu.edu

ABSTRACT

The rapid decrease in the critical current density J_c with grain boundary (GB) misorientation angle θ strongly limits the current-carrying capability of yttrium–barium–copper-oxide (YBCO), and the residual *low-angle* GB distribution is the most important current-limiting mechanism in biaxially textured YBCO coated conductors. To deepen the understanding of the Ca doping in low-angle GBs in YBCO, transport characteristics of low-angle GBs in $YBa_2Cu_3O_{7-d}$ bicrystals with different Ca contents x ($Y_{1-x}Ca_xBa_2Cu_3O_{7-d}$) were examined to verify the influence of the carrier density at the GB due to the Ca doping level. $Y_{1-x}Ca_xBa_2Cu_3O_{7-d}$ (x = 0, 0.10, 0.15, and 0.30) epitaxial films were deposited by pulsed laser deposition on single crystal $SrTiO_3$ (STO) substrates and 7° and 9° symmetric [001]-tilt bicrystal STO substrates. We found that 15% Ca doping was the most effective at increasing the J_c behavior across the 7° GB in intermediate fields, completely eliminating the GB dissipation signature in the *V–I* characteristics. For the 9° GB, 10% Ca doping yielded the highest depairing current J_d across the GB, calculated from the flux flow resistivity, even though a significant GB dissipation signature remained in the *V–I* curves.

Published under license by AIP Publishing. https://doi.org/10.1063/5.0016157

I. INTRODUCTION

The rapid decrease in the critical current density J_c with the grain boundary (GB) misorientation angle θ limits the current-carrying capability of yttrium–barium–copper-oxide (YBCO) coated conductors (CC).[1–5] Although the in-plane texture of YBCO coated conductors (CCs) has been greatly improved, generally to 4°–6° of the full-width at half-maximum (FWHM), previous studies of the current-limiting mechanisms of the GB network in real CCs have shown that even the very best textured-substrate CCs have low-field J_c properties that are limited by the low-angle GB network.[6,7] Thus, residual low-angle GBs ($\theta \sim 5°$–10°) are still a very important current-limiting mechanism in YBCO CCs. In addition, the influence of GB effects becomes very significant when the tape is subdivided into narrow bridges to reduce AC losses.[6] Since most electric utility applications use fields less than 3 T and are expected to operate in AC conditions, the enhancement of low-angle GB properties will always be very valuable.

Low-angle GBs are composed of an array of alternating superconducting channels and weakly superconducting, under-doped, or even insulating GB dislocation cores.[8] The off-stoichiometric compositions and lattice distortions around the GB dislocation cores reduce the channel hole–carrier density and modify the electronic structure within a few nm of the GB cores. Indeed, carrier-depletion layers were experimentally observed by electron energy loss spectroscopy (EELS),[9,10] suggesting that it should be possible to enhance the GB transparency by hole-doping, Ca substitution,[11,12] or oxygen annealing.[13] The beneficial effects on J_c across the GB ($J_{c,gb}$) of doping by partial substitution of Ca^{2+} for Y^{3+} in $YBa_2Cu_3O_{7-d}$ were first demonstrated by the Augsburg group, especially for 24° and 36° high-angle grain boundaries.[11,12] An optimum replacement of Y by substitution of 30% Ca at 4.2 K (to make the composition $Y_{0.7}Ca_{0.3}Ba_2Cu_3O_{7-d}$) was determined for the high-angle grain boundaries (mainly 24° [001] tilt). Shortly afterward, it was shown that $J_{c,gb}$ for a 5° [001] tilt low-angle GBs could be significantly improved by 30% Ca doping as well.[13]

Published under license by AIP Publishing.

There has been some effort to better understand how Ca doping influences the intergrain $J_{c,gb}$ of $Y_{1-x}Ca_xBa_2Cu_3O_{7-d}$. Significant reduction of the excess charge at the grain boundary was indeed revealed by comparative electron holography of 4° [001]-tilt pure and 30% Ca-doped YBCO bicrystals for which the negative GB potential was smaller (−1 vs −2.4 V) and decayed over a shorter length (0.8 vs 1.7 nm) for the Ca-doped GB.[14] Klie *et al.*[15] reported that highly strained grain boundary regions contain excess oxygen vacancies, which reduce the hole concentration at the boundary. They claimed agreement between Z-contrast scanning transmission electron microscopy (STEM) images, electron energy loss spectroscopy (EELS), and density functional theory (DFT) calculations, concluding that excess holes introduced by Ca^{2+} substitution for Y^{3+} do not much improve the GB properties. By density functional theory (DFT) modeling, they concluded that Ca^{2+} ions can replace Y^{3+} in intra-grain Y(Ca)BCO, but that Ca^{2+} also tends to replace large Ba^{2+} ions in the compressed regions of the dislocation core, and the smaller Cu^{2+} ions in the tensile regions of the dislocation cores. Thus, the Ca^{2+} substitutions relieve the GB strain and also suppress O vacancy formation. They suggested that dopants should be selected for their size, more than just for their valence, proposing Eu and Ag as good candidates. The interesting picture that emerges from these studies is that there are strong driving forces for segregation to [001] tilt grain boundaries that may enable the improvement of grain boundary properties without incurring the marked depression of T_c that occurs by Ca addition.

Concurrently with the Klie *et al.* study, Song *et al.*[16] were investigating the lattice structure, electronic state, and current transport of pure and Ca-doped GBs in low-angle YBCO bicrystals by combining measurements of the extended voltage–current (V–I) characteristics on a matched pair of 30% Ca-doped and pure 7° [001]-tilt YBCO bicrystals with detailed atomic-scale microscopy of exactly the same GBs. Most unexpectedly, they found that Ca-doped grain boundaries had greatly expanded dislocation cores, which narrowed the "undisturbed" channel between the dislocations. A very significant Ca segregation (50% enhancement) at the GB cores and a strong non-monotonic variation of Ca concentration along the GB plane and across the dislocation cores were observed. This segregation occurred on scales of ∼1 nm that matched the core-channel structure of the grain boundary. In spite of a clearly observed expansion of the dislocation cores normal to and parallel to the grain boundary and shrinking of the channel, surprisingly, $J_{c,gb}$ significantly increased, approaching the critical current density in the grains. To explain this behavior, a cation segregation model was proposed in which Cottrell atmospheres of Ca ions[16] formed under the combined strain[15,16,18] and electric fields of the dislocations[19,20] making up a low-angle grain boundary. In this model, the driving force for Ca segregation is then due to both *size* and *valence difference* between Y^{3+} and Ca^{2+}. The Ca^{2+} segregation at the GB dislocation core produces an enhanced charge carrier density (holes) both by the substitution and by the strain relief produced by expanding the core, thus causing the transport properties to change according to the Ca doping level. Recently, Li *et al.*[21] investigated the transport characteristics of low-angle GB in a series of Ca-doped $YbBa_2Cu_3O_{7-d}$ (Yb is a smaller rare earth ion than Y) over a wide temperature, field, and field orientation using low-temperature scanning laser microscopy[22] and magneto-optic imaging.[23] They determined that $J_{c,gb}$ can even exceed the intragrain J_c at high field and low temperature where the pinning by GB dislocations can be optimized.

Based on earlier experimental Ca doping studies on high-angle GBs, it was generally believed that 30% Ca is the optimum doping level for improvement of grain boundary transparency. However, the segregation model[16,17] predicts that the optimum concentration should depend on the misorientation angle. In this paper, lower levels of Ca substitution were explored for the lower angle (7° and 9°) GBs occasionally found in CCs. Thus, the purpose of the present paper is to deepen our understanding of the influence of Ca doping on low-angle grain boundaries in YBCO by study of low-angle bicrystal thin films. Transport characteristics of low-angle GBs (7° and 9°) with different Ca contents x ($Y_{1-x}Ca_xBa_2Cu_3O_{7-d}$) were examined to verify the influence of the GB carrier density due to the Ca doping level. We amplified our study by interpreting the transport characteristics of Ca-doped low-angle grain boundaries based on the cation segregation model of Gurevich.[16] Broad-range measurements of $J_c(H,T)$ and the voltage–current (V–I) characteristics of a series of variable Ca doping levels in 7° and 9° bicrystals were performed and are discussed. We found that Ca additions can strongly benefit $J_{c,gb}$ at intermediate fields near T_c and at a reduced temperature $t = T_m/T_c \sim 0.85$, where T_m is the measurement temperature and T_c is the critical temperature, which corresponds to 77 K for T_c of ∼90 K. This, we hope, enables a proper comparison between the undoped and doped films with different T_c. Since the Ca doping is accompanied by T_c reduction due to over-doping of the grains, the improvement was measured at $t = 0.85$ in all cases. We found that 15% Ca doping is most effective in increasing J_c for a 7° [001]-tilt GB, completely eliminating the GB signature in the V–I characteristics. In addition, the flux flow resistivity was calculated for the 9° GB and we found that 10% Ca doping produced the highest grain boundary depairing current $J_{d,gb}$. We also showed that full oxygenation produced a relative enhancement of $J_{c,gb}(H)$ at the reduced temperature $t \sim 0.85$, even though it drove the Ca-doped sample to lower T_c.

II. SAMPLE PREPARATION AND EXPERIMENTAL DETAILS

$Y_{1-x}Ca_xBa_2Cu_3O_{7-d}$ (x = 0, 0.10, 0.15, and 0.30) films were deposited on single crystal $SrTiO_3$ (STO) substrates and 7° and 9° symmetric [001]-tilt bicrystal STO substrates by pulsed laser deposition (PLD). The substrate temperature during growth was set at 800–810 °C, while the oxygen pressure was set to 200 mTorr during growth. Films were deposited with ∼500 nm thickness using 7000 pulses at 5 Hz. The films were post-annealed in oxygen at 475–500 °C for 2 h. The undoped sample was annealed at 800 Torr to allow full oxygenation, but the Ca-doped samples were annealed at the lower oxygen pressures of 15–200 Torr listed in Table I, so as to achieve the highest T_c for each Ca content.[24] Full oxygenation of the Ca-doped samples would have reduced the T_c too much, degrading our J_c(H) property comparison at constant reduced T_c. After T_c and $J_c(H,T)$ measurement, some samples were further oxygenated at 800 Torr to establish fully oxygenated (i.e., strongly overdoped) states and were compared to the samples that were annealed at lower oxygen partial pressures to achieve maximum T_c.

Published under license by AIP Publishing.

TABLE I. Summary of the T_c of each sample and its annealing condition for maximum T_c.

O_2 annealing condition	0% Ca 800 Torr	10% Ca 200 Torr	15% Ca 15 Torr	30% Ca 15 Torr
T_c (Intra-grain)	90.2 K	80.1 K	81.6 K	84.0 K
T_c (7° GB)	87.6 K	77.1 K	81.1 K	83.6 K
T_c (9° GB)	88.3 K	79.3 K	82.5 K	84.6 K

Transport measurement bridges were cut to 40 μm (width) × 1000 μm (length) using a Nd–YAG (yttrium aluminum garnet) laser cutter. The V–I characteristics were obtained with standard four-point measurements using a current reversal algorithm to remove thermal voltage effects. All measurements were made at the same reduced temperature $t \sim T_m/T_c$ of 0.85 (which corresponds to 77 K for pure and fully oxidized YBCO) for better comparison, since the T_c varies according to the Ca content and oxygen annealing condition.[25] A current pulse of 50 ms duration with a 30 ms voltage read window was used for currents higher than 100 mA to prevent sample heating. The measurements were performed over a wide range of magnetic fields up to 12 T applied perpendicular to the film surface in a superconducting magnet system. The J_c values were determined using an electric field criterion of 1 μV/cm. The irreversibility field $\mu_0 H_{irr}$ was defined where J_c becomes 100 A/cm^2. The grain boundary depairing current density was deduced by measuring the flux flow resistance $R_F(H)$ of the GB in bicrystals as a function of the magnetic field. The relative orthorhombicity of the films was measured by two-axis ω–$\omega/2\theta$ scans near the [101] STO and [103] YBCO diffraction peaks using a 2D GADDS area detector.

III. RESULTS

A. Optimum Ca doping in 7° [001]-tilt grain boundary

Figures 1(a) and 1(b) show $J_c(H)$ and the $J_c(h = H/H_{irr})$ plots at reduced field of $Y_{1-x}Ca_xBa_2Cu_3O_{7-d}$ (x = 0, 0.10, 0.15, and 0.30) for 7° [001]-tilt GB for samples annealed to have maximum T_c (Table I). To better compare the transport characteristics between samples with different T_c, the J_c characteristics were measured at the same reduced temperature $t = T_m/T_c$ of ∼0.85, which corresponds to 77 K for fully oxidized YBCO but is always lower for the Ca-doped samples. A reduced field, $h = H/H_{irr}$, was also used for comparison purposes in some cases [Fig. 1(b)]. The 30% Ca substitution exhibited a severe reduction of $J_{c,gb}$ over the entire field range up to $\mu_0 H_{irr}$, while the 10% and 15% Ca substitutions showed significant enhancements of $J_{c,gb}$ in intermediate fields higher than ∼0.2 T and then at all fields up to $\mu_0 H_{irr}$. The data clearly indicate an improvement of $J_{c,gb}$ at intermediate fields for intermediate Ca doping, with 10% and 15% Ca clearly being the best. Figures 1(c)–1(f) show the corresponding V–I characteristics for the $J_c(H)$ measurement. The pure (0% Ca) 7° GB showed a typical GB kink with a steep voltage rise and a knee at higher voltages on a log–log V–I plot [Fig. 1(c)]. The steep voltage rise in the pure and 30% Ca-doped bicrystals is the characteristic GB dissipation signature caused by depinning of hybrid Abrikosov–Josephson (AJ) vortices in the GB.[26] However, the GB kink in the V–I characteristics became weaker at 10% Ca doping and disappeared at 15% Ca doping [Figs. 1(d) and 1(e)]. This result agrees with the $J_c(H)$ and $J_c(h)$ results in Figs. 1(a) and 1(b), which exhibited $J_{c,gb}$ improvements for 10% and 15% Ca doping at intermediate fields. By contrast, 30% doping of the 7° GB degraded the GB properties significantly, as is seen in Figs. 1(a) and 1(f).

However, $J_{c,gb}$ was reduced at self-field and low fields (< ∼ 0.2 T) for all Ca substitutions [Fig. 1(a)], a consequence of the reduced intra-grain vortex pinning produced by Ca substitutions. Figure 2 exhibits $J_c(H)$ and $J_c(h)$ of single crystals (intra-grain) of pure and Ca-doped YBCO. The J_c reduction is also seen for 10% and 15% Ca-doped samples at fields less than around 1 T. Otherwise, the absolute $J_c(H)$ in Fig. 2(a) and the reduced $J_c(h)$ characteristics in Fig. 2(b) of the 0%, 10%, 15% Ca-doped samples overlap well at fields greater than ∼1 T (or a reduced field h of ∼0.1) even though there is slight variation of $\mu_0 H_{irr}$ [Fig. 2(a)], while the 30% Ca-doped sample exhibited a dramatic reduction in J_c and $\mu_0 H_{irr}$. Figure 3 shows two-axis XRD scans around [103] for Ca-doped YBCO on single crystal STO optimized for maximum T_c. The Ca substitution reduces the orthorhombicity compared to the pure YBCO lattice [note that the four symmetric YBCO [103] peaks that appear as an X shape in Fig. 3(a) shift closer together in Figs. 3(b)–3(d), being more or less one peak in Fig. 3(b)]. The increase of the orthorhombicity in Figs. 3(c) and 3(d) at 15% and 30% Ca doping would be due the progressive oxygen deficiency. The 10% Ca shows the least orthorhombicity and also exhibits the smallest J_c at the self-field and low fields. Smaller orthorhombicity may reduce the twin density and vortex pinning that crystal twinning introduces and is likely the cause of the reduced low-field intra-grain J_c reduction.

Figures 4(a) and 4(b) show the reduced $J_c(h)$ plot and the V–I characteristics at $t \sim 0.85$ of the 7° [001]-tilt GB, 15% Ca-doped sample after full oxygenation (annealed at 800 Torr). The T_c was further reduced from 81.1 K to 70.8 K after full oxygenation. The $\mu_0 H_{irr}$ after full oxygenation rose to 6.9 T from the value of 5.3 T of the maximum T_c optimally doped sample. The magnitude of J_c was further enhanced by full oxygenation compared to J_c in the maximum T_c state. Like the maximum T_c sample [Fig. 1(e)], the V–I characteristics of the fully oxygenated 15% Ca-doped sample [Fig. 4(b)] do not exhibit any GB dissipation signature.

B. Ca doping of 9° [001] tilt grain boundaries and their flux flow behavior

Figures 5(a) and 5(b) show absolute $J_c(H)$ and reduced $J_c(h)$ of $Y_{1-x}Ca_xBa_2Cu_3O_{7-d}$ ($x = 0$, 0.10, 0.15, and 0.30) for 9° [001] tilt grain boundaries at $t \sim 0.85$. These samples were oxygen-annealed for maximum T_c (Table I). 30% Ca doping produced a severe reduction of $\mu_0 H_{irr}$ from ∼7 to ∼2 T [Fig. 5(a)]. Although different Ca levels exhibited similar $J_c(h)$ behaviors, the 10% and 15% Ca-doped bicrystals exhibited a small J_c increase, with the 10% sample being the best in intermediate fields [Fig. 5(b)]. As seen in Figs. 5(c)–5(f), the large GB signature in the V–I curves was observed despite the Ca doping. Thus, there is a marked difference between the behaviors of the 7° and 9° Ca-doped bicrystals, Ca clearly bringing no benefit for the 9° GB.

Published under license by AIP Publishing.

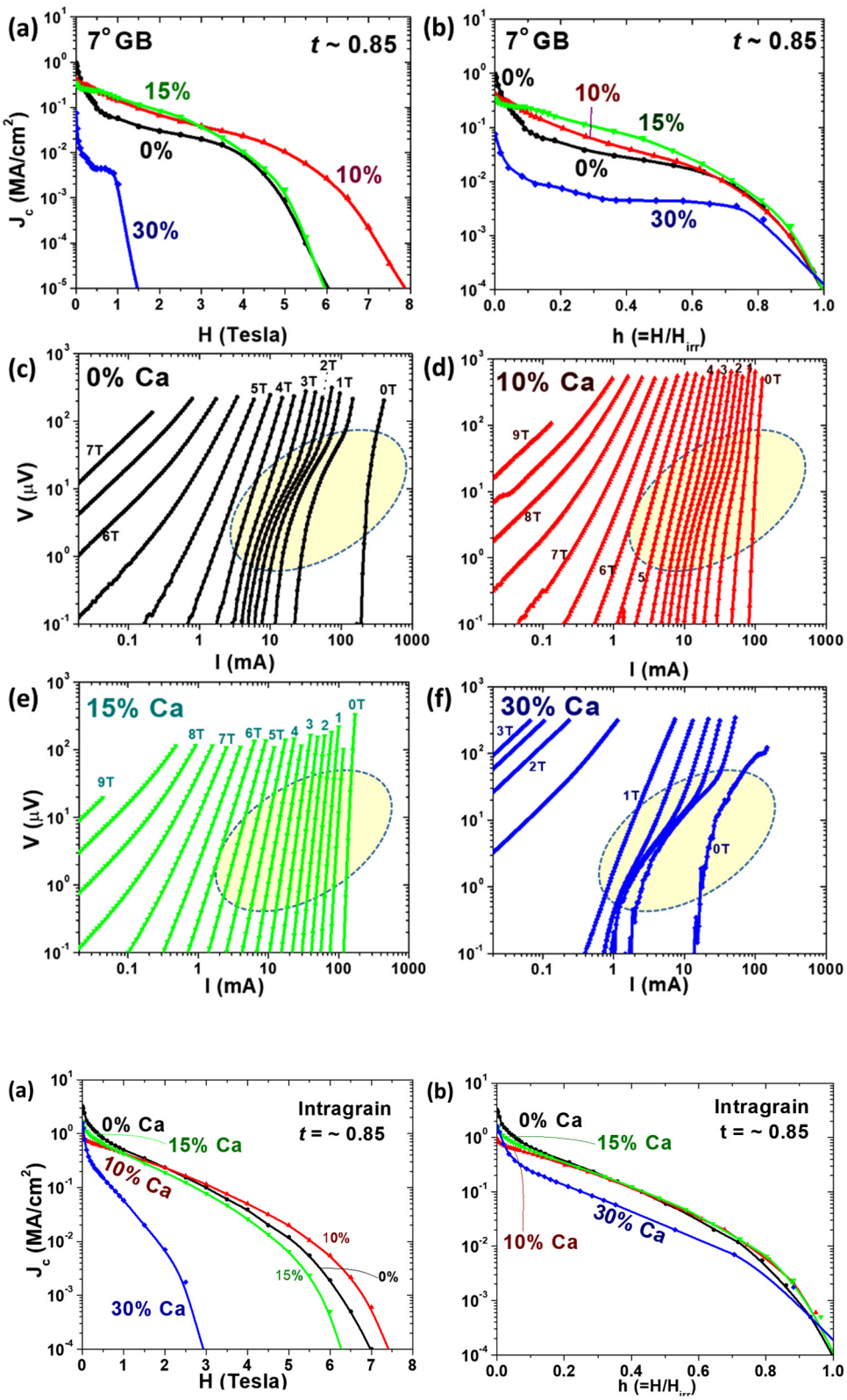

FIG. 1. (a) $J_c(H)$ and (b) reduced $J_c(h = H/H_{irr})$ of $Y_{1-x}Ca_xBa_2Cu_3O_{7-d}$ (x = 0, 0.10, 0.15, and 0.30) for 7° [001]-tilt grain boundary. The samples were annealed for the maximum T_c (Table I). $J_c(h)$ was measured at the same reduced temperature of $t = T_m/T_c \sim 0.85$ for comparison. The 10% and 15% Ca bicrystals show increases in J_c in intermediate fields, while the 30% Ca-doped sample exhibits a substantial J_c reduction in the entire field range. *V–I* curves of $Y_{1-x}Ca_xBa_2Cu_3O_{7-d}$ for x of (c) 0, (d) 0.10, (e) 0.15, and (f) 0.30 for the 7° grain boundary. (c) and (f) show a typical GB signature, which appears as a knee-shape of the curves. However, the GB signature was significantly reduced for (d) 10% Ca-doped YBCCO and is absent for the (e) 15% Ca-doped YBCO.

FIG. 2. (a) $J_c(H)$ and (b) $J_c(h = H/H_{irr})$ plot at reduced field of intra-grain of Ca-doped YBCO. Other than the 30% Ca sample, the curves overlap well at fields greater than 1 T (or a reduced field h of ~0.1) even though there is slight variation of the irreversibility field $\mu_0 H_{irr}$. The 30% Ca doping sample exhibits a dramatic reduction in $\mu_0 H_{irr}$.

Published under license by AIP Publishing.

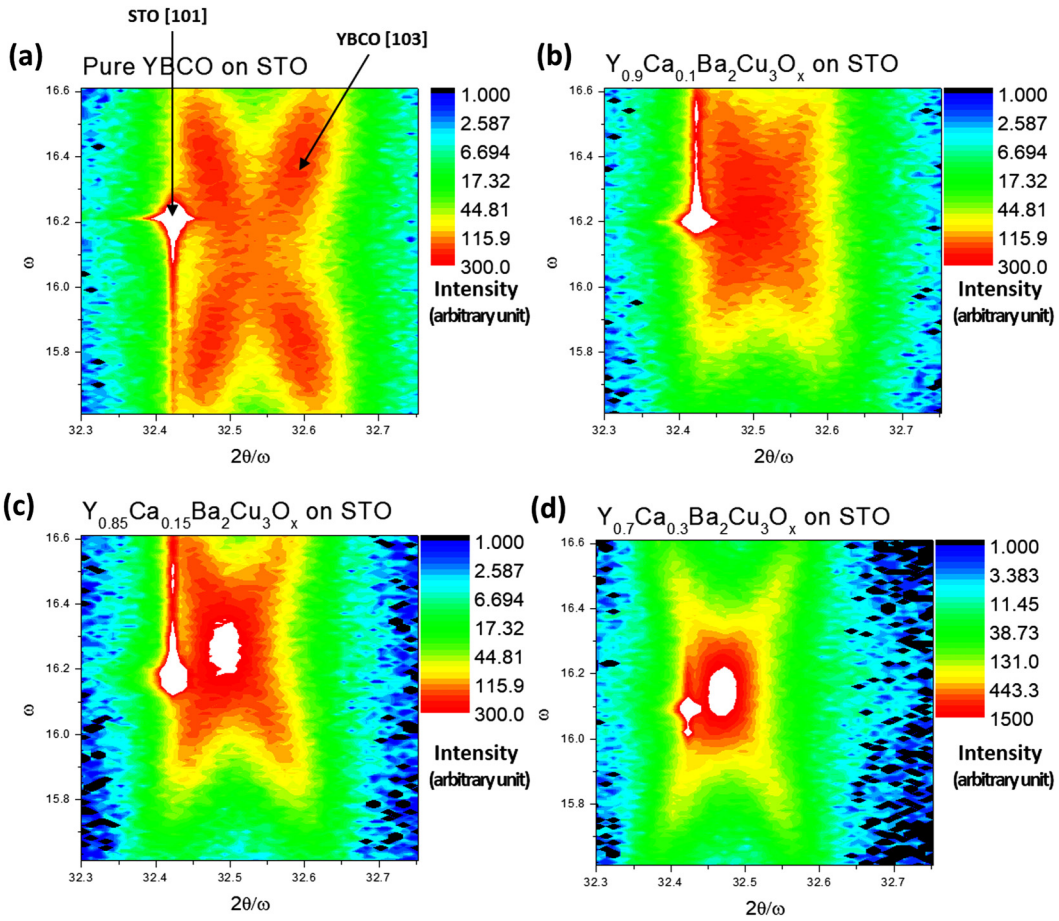

FIG. 3. Two-axis (ω–$\omega/2\theta$) scans near [101] STO and [103] YBCO space for (a) pure YBCO, (b) 10% Ca-, (c) 15% Ca-, and (d) 30% Ca-doped YBCO optimized to maximum T_c are shown. The pure YBCO results indicate a distinctive orthorhombicity, while the orthorhombicity reduces as Ca is added.

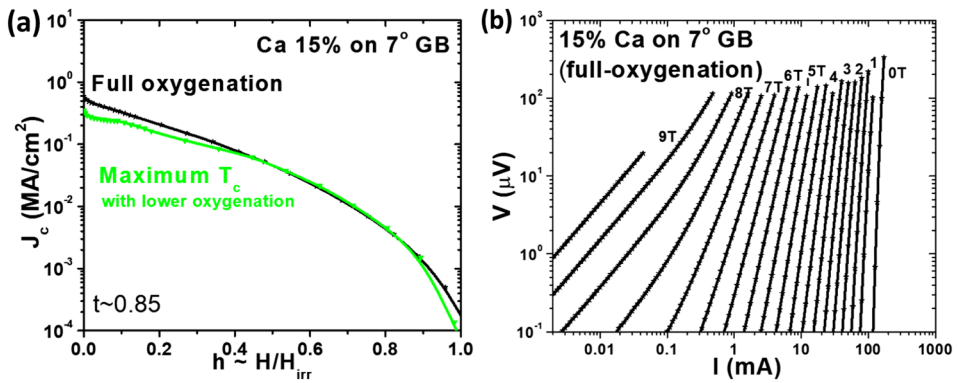

FIG. 4. (a) $J_c(h)$ plot at reduced field for 7° [001]-tilt GB for 15% Ca doping for sample of two different oxygenation states. One sample was oxygenated in 15 Torr O_2 to achieve the maximum T_c and the other in 800 Torr O_2 to achieve a fully oxygenated state. The magnitude of J_c was further enhanced by the full oxygenation. (b) V–I curves across the 15% Ca-doped YBCO 7° GB for the fully oxygenated sample. No GB dissipation signature is observed. The detailed shape of these curves can be compared to Fig. 1(e), which is the V–I curves across the 15% Ca-doped YBCO 7° GB maximum T_c state.

Published under license by AIP Publishing.

In the 9° bicrystals, it was possible to calculate the core size l of the AJ vortices (along the GB) for the various Ca-doped 9° GBs, since the GB dissipation signature was always present [Figs. 5(c)–5(f)]. Thus, the flux flow resistances $R_F(H)$[26] were calculated (see the supplementary material for details) based on the linear dissipation (flux flow resistance) regimes in the linear V, linear I characteristics of Figs. 6(a)–6(d). A summary of these $R_F(H)$ values is plotted in Fig. 6(e) and the output of the calculations is shown in Table II. For pure YBCO, the AJ vortex core size was calculated as 39 nm from equation (S2) in the supplementary material, which shows that the AJ vortex size was much larger than the coherence length $\xi \sim 4$ nm but much smaller than the London penetration depth $\lambda \sim 400$ nm.[26] For 10%, 15%, and 30% Ca, the core sizes were reduced to 23, 27, and 32 nm, respectively, compared to 39 nm of the pure YBCO 9° GB. Here, the AJ vortex core size for the 10% Ca-doped YBCO sample on the 9° GB was the smallest. Since the grain boundary depairing current density, $J_{c,gb}$, is inversely proportional to the AJ vortex core size as calculated form equation (S2) in the supplementary material, the 10% Ca-doped YBCO GB showed the best $J_{d,gb}$ of 0.17 J_d ($J_d \sim$ intra-grain depairing critical current density, Table II). This proves that Ca doping does reduce the AJ vortex core size, enhancing $J_{d,gb}$, by allowing stronger pinning of AJ vortices. For the 9° samples, 10% Ca doping was the most effective, although significant GB dissipation was always present. The 9° bicrystals were then fully oxygen-annealed to test the influence of oxygen over-doping, and their $J_c(h)$ values at $t \sim 0.85$ are plotted in Fig. 7. The T_c values were 88.3, 79.4, 71.9, and 64.6 K, and their corresponding $\mu_0 H_{irr}$ were 6.9, 7.2, 6.3, and 1.6 T for 0%, 10%, 15%, and 30% Ca doping, respectively. In Fig. 7, the 10% Ca exhibited the best properties over the entire regime, in accordance with its highest depairing current $J_{d,gb}$ and smallest calculated core size.

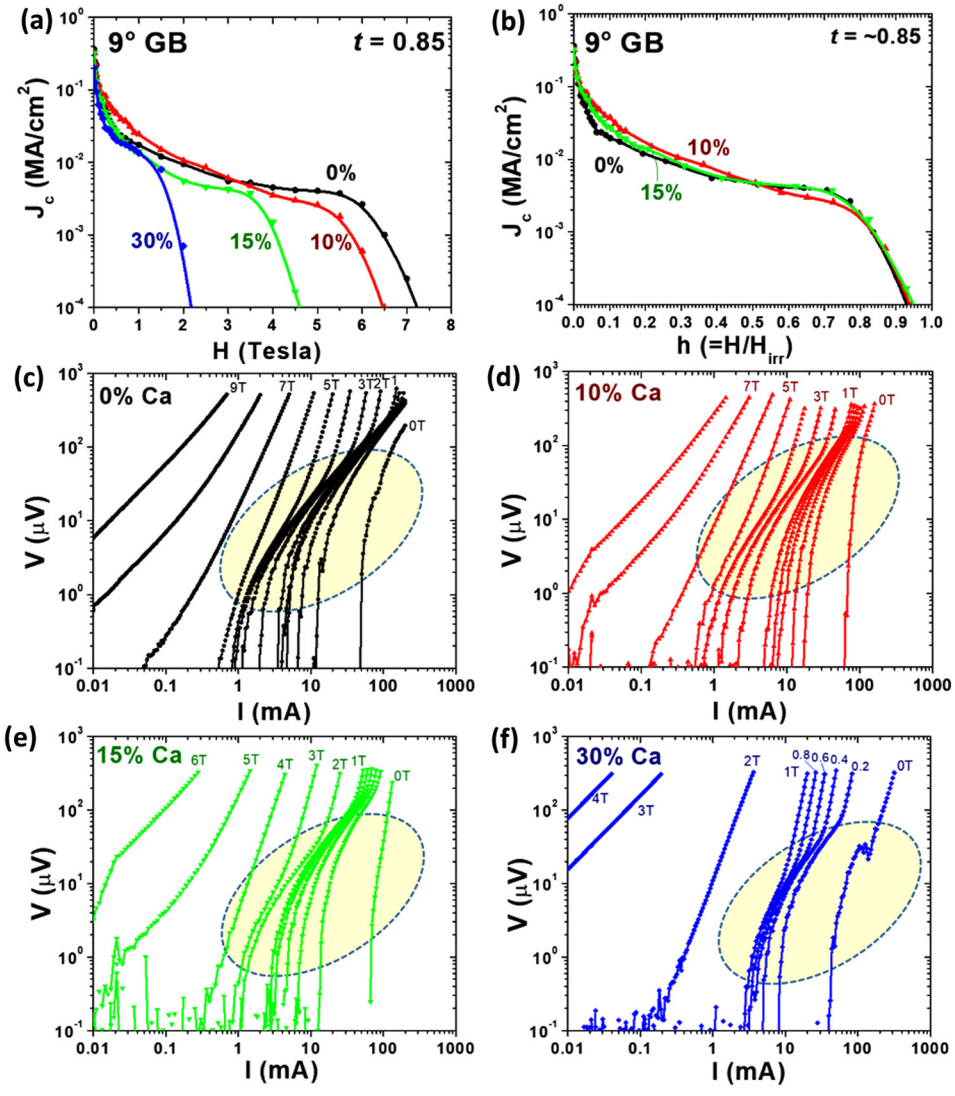

FIG. 5. (a) $J_c(H)$ and (b) the $J_c(h = H/H_{irr})$ plot at reduced field of $Y_{1-x}Ca_xBa_2Cu_3O_{7-d}$ (x = 0, 0.10, 0.15, and 0.30) for the 9° [001]-tilt grain boundary. V–I curves of $Y_{1-x}Ca_xBa_2Cu_3O_{7-d}$ for x of (c) 0, (d) 0.10, (e) 0.15, and (f) 0.30 for 9° grain boundary. All V–I curves exhibit significant GB dissipation signatures.

Published under license by AIP Publishing.

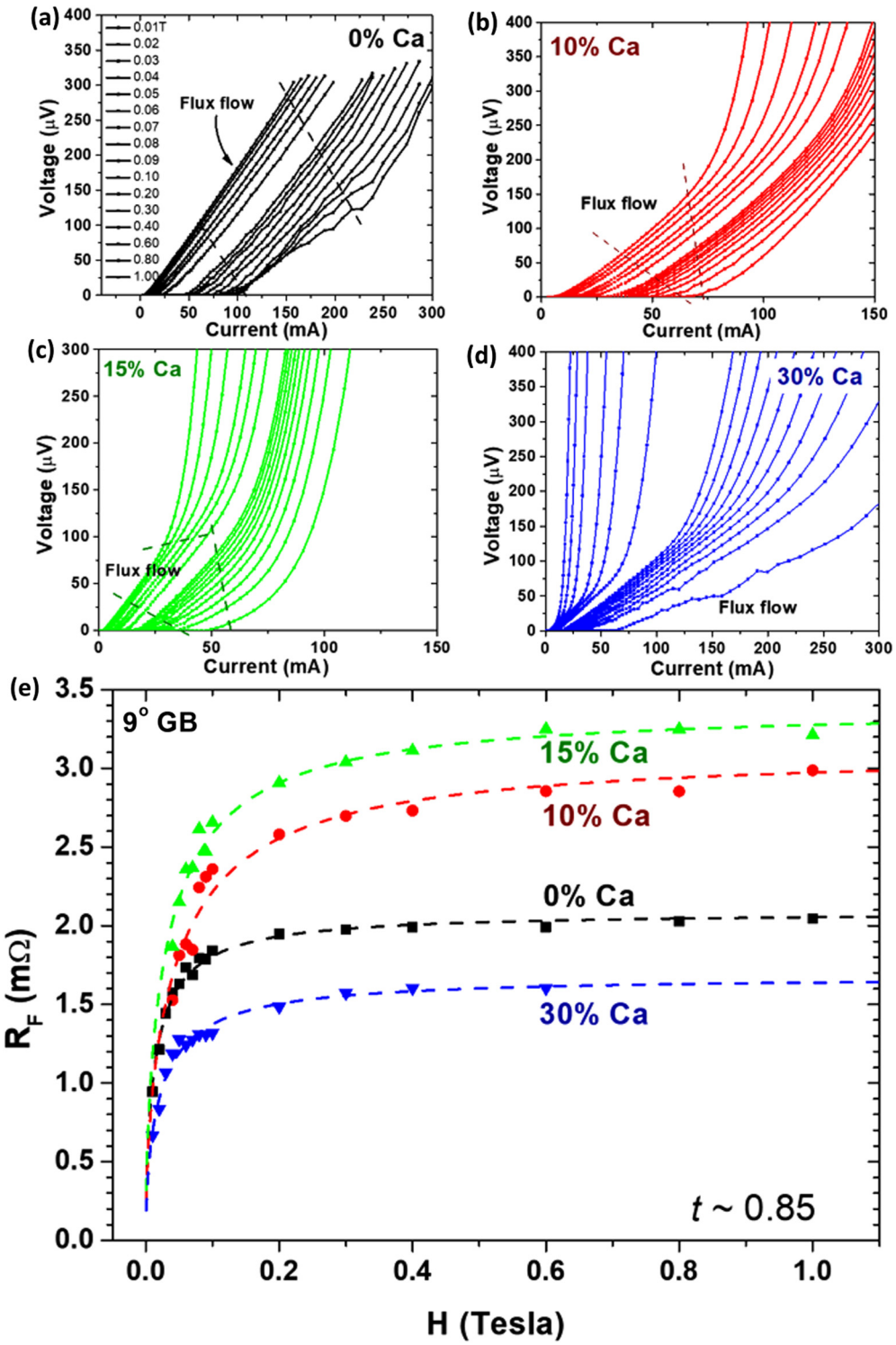

FIG. 6. *V–I* curves in a linear–linear plot across a 9° grain boundary of (a) pure, (b) 10% Ca-doped, (c) 15% Ca-doped, and (d) 30% Ca-doped YBCO are shown. Flux flow behavior of the vortices is seen in all the samples. (e) Summary of $R_F(H)$ for of $Y_{1-x}Ca_xBa_2Cu_3O_{7-d}$ for x ~ 0, 0.10, 0.15, and 0.30.

Published under license by AIP Publishing.

TABLE II. Calculated H_0, l, and $J_{d,gb}$ values for each Ca-doped 9° [001]-tilt GB from $R_F(H)$ data.

Ca content	H_0	l	$J_{d,gb}$
0%	34 mT	39 nm	0.10 J_d
10%	97 mT	23 nm	0.17 J_d
15%	72 mT	27 nm	0.15 J_d
30%	49 mT	32 nm	0.13 J_d

IV. DISCUSSION

The present report presents detailed experimental results on the transport behavior of 7° and 9° low-angle GBs and their dependence on Ca doping level (0%, 10%, 15%, and 30%). Improved $J_{c,gb}$, weaker superconductivity depression and weaker (or no) GB dissipation signature were seen at some Ca-doped low-angle GBs, evaluated at a constant T/T_m of 0.85 equivalent to 77 K for pure YBCO.

A key issue for understanding the influence of Ca doping on the low-angle GBs is to understand the segregation of Ca as a function of the misorientation angle. Thus, the Ca distributions near the GB cores for each Ca content were calculated for the 7° GBs based on the cation segregation model,[17] and the results are plotted in Figs. 8(a)–8(c). Details of the model are described in the supplementary material. The same parameters used in Ref. 16 were adapted for the calculations, while only the Ca doping level and the misorientation angles were modified. The Ca segregation is predicted to occur at the dislocation cores on scales of a few nm. Ca-depleted regions are also predicted between the cores and

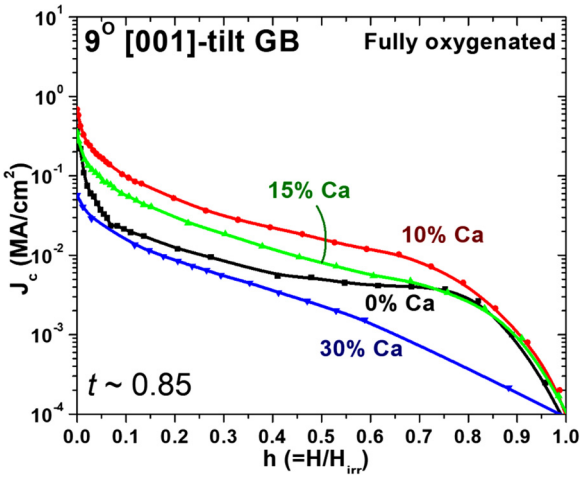

FIG. 7. The $J_c(h)$ plot at reduced field of fully oxygenated $Y_{1-x}Ca_xBa_2Cu_3O_{7-d}$ (x = 0, 0.10, and 0.30) for the 9° [001]-tilt grain boundary. $J_c(h)$ was measured at the same reduced temperature of ~0.85 for comparison.

evidence for higher T_c channels were deduced by Li *et al.*[21] For the 10% Ca-doped GB [Fig. 8(a)], the peak Ca segregation is ~20%, which is insufficient for optimum doping. As a small GB signature was observed, ellipsoidal vortices representing the AJ hybrid vortices are illustrated at the bottom of Fig. 8(a). In the 15% Ca-doped GB [Fig. 8(b)], the peak Ca concentration is ~28%, about twice the

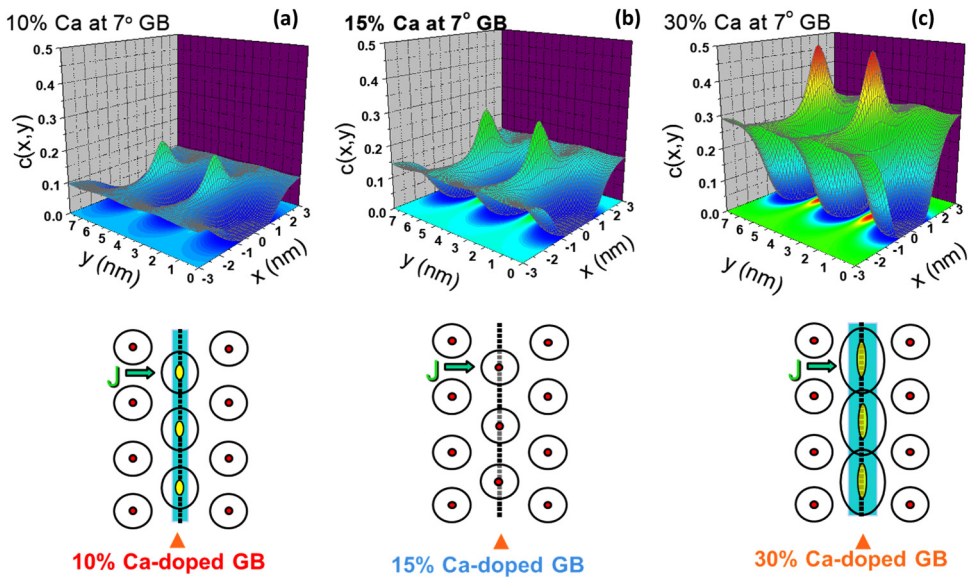

FIG. 8. The calculated Ca distribution near the grain boundary cores from the cation segregation model are shown for (a) 10%, (b) 15%, and (c) 30% Ca-doped samples. The bottom illustrations represent the expected vortex array near and along the GB. The round vortices correspond to Abrikosov vortices, while the ellipsoidal vortices correspond to the Abrikosov–Josephson hybrid vortices.

Published under license by AIP Publishing.

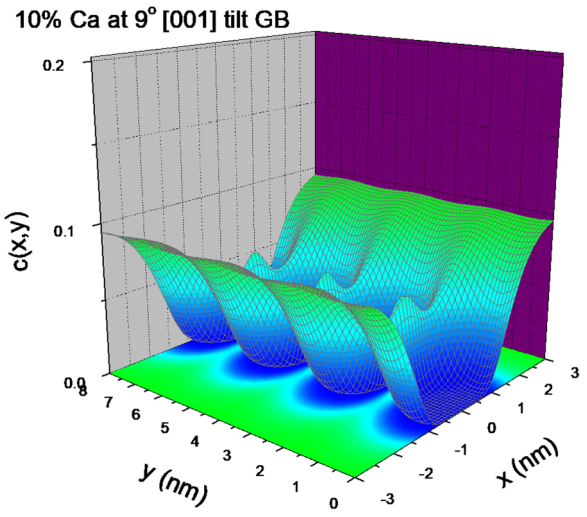

FIG. 9. The calculated Ca distribution near the grain boundary cores from the cation segregation model are shown for 10% Ca-doped 9° GB.

bulk level, sufficient to induce A vortices,[26] consistent with our transport results.

The Ca distribution occurring in the 15% doped 7° [Fig. 8(b)] appears optimal. The 30% Ca doping may have induced too much segregation (>45%), because the sample exhibited a $J_{c,gb}$ that was not better than those of the 10% or 15% Ca-doped samples. Therefore, it is clearly shown that the optimum Ca doping depends on the misorientation angle. We note that earlier studies considered 30% Ca doping to be optimal for GBs in YBCO judged by earlier studies on high-angle GBs.[11,12]

In contrast to the beneficial effects of Ca doping of the 7° GB, Ca doping of the 9° GB does not significantly enhance $J_{c,gb}$ nor eliminate the GB dissipation signature in the V–I characteristics. However, the 10% Ca sample exhibited the highest J_c. Thus, there is a distinctive difference between the 7° and 9° GBs. From the segregation model calculation, desegregation of Ca at the dislocation core (compared to the intra-grain) was anticipated at the 9° GB, as seen in Fig. 9 (which plots the Ca-level for the 10% Ca-doped 9° GB). This may indicate that the beneficial influence of Ca for low-angle GBs is only valid for angles less than 9°. The present study thus provides a better understanding of the cation segregation effects around low-angle GB cores and its influence on the transport properties. The cation segregation model[17] appears to be valid for interpreting the transport characteristics of our measured 7° and 9° GBs.

Further oxygen annealing enhances $J_{c,gb}(H)$ at $t \sim 0.85$ (Fig. 4 for 7° GB and Fig. 7 for 9° GB). The results suggest that oxygen over-doping benefits the transparency of the GB by adding additional carriers at the GB. As seen in Fig. 7, an improvement of the $J_c(h)$ behavior by Ca doping is apparent in the fully oxygenated samples, in contrast to the $J_c(h)$ behaviors of the optimum T_c samples [Fig. 5(b)]. For fully oxygenated samples, 10% and 15% Ca doping of the 9° GB produced much higher $J_{c,gb}$ values than the undoped 9° GB in intermediate fields, agreeing with the core size calculation (Table II).

Although we found that the Ca doping improves the GB transport properties for low-angles, it is accompanied by a substantial decrease in T_c due to Ca over-doping of the YBCO grains, a fact not always obvious in the way that we have plotted the data since we chose make our comparisons at the same reduced temperature $t = T_m/T_c \sim 0.85$. An approach to remedy the T_c depression effect of Ca is still required.

The other drawback of Ca doping that we found is that the Ca doping reduces the orthorhombicity of YBCO, as seen in Fig. 3, apparently reducing native vortex pinning defects, like twins. As a result, only the self-field and low-field J_c values were reduced. However, insulating precipitates, such as Y_2O_3, $BaZrO_3$, or Y_2BaCuO_5, can enhance pinning in both low and high fields in YBCO.[27,28] Thus, lowering of the orthorhombicity does not invalidate Ca doping as an approach to ameliorating the GB properties, since nanoparticle intra-grain pinning can be used to optimize pinning in the grain.[27,28]

V. CONCLUSION

We examined low-angle GBs with different Ca contents x ($Y_{1-x}Ca_xBa_2Cu_3O_{7-d}$) and different misorientations (7° and 9°) and demonstrated that Ca additions can strongly benefit the $J_{c,gb}$ behavior at intermediate fields and high reduced temperatures $t = T_m/T_c \sim 0.85$, which corresponds to 77 K for pure YBCO. It was found that 15% Ca doping was the most effective at enhancing GB transparency for a 7° GB in YBCO. The V–I characteristics showed no sign of GB dissipation, which suggests the possibility of removing grain boundary effects in CC and, very desirably, achieving single-crystal-like properties. The loss of the GB dissipation signature at 15% Ca doping indicates that the critical current is no longer limited by GBs but becomes limited by intra-grain vortex pinning. For the Ca-doped films with 9° GBs, it was found that the smallest AJ vortex core size and the highest grain boundary depairing current $J_{d,gb}$ occurred at 10% Ca doping. Although the T_c depression due to Ca doping is still problematic, the results suggest significant new opportunities for nanoscale cation segregation engineering based on the *size* and *valence differences* in low-angle GBs.

SUPPLEMENTARY MATERIAL

See the supplementary material for the description of the cation segregation model and flux flow behavior at gain boundary.

ACKNOWLEDGMENTS

This work was supported by the Air Force Office of Scientific Research at the National High Magnetic Field Laboratory in Tallahassee, FL, which is also supported by the National Science Foundation under Cooperative Agreement Nos. DMR-0654118 and DMR-1644779, by the State of Florida, and by the Basic Science Research Program through the National Research Foundation of Korea (NRF) (No. NRF-2019R1C1C1005254).

Published under license by AIP Publishing.

DATA AVAILABILITY

The data that support the findings of this study are available from the corresponding author upon reasonable request.

REFERENCES

[1]D. Dimos, P. Chaudhari, and J. Mannhart, Phys. Rev. B **41**, 4038 (1990).
[2]D. M. Feldmann, D. C. Larbalestier, D. T. Verebelyi, W. Zhang, Q. Li, G. N. Riley, R. Feenstra, A. Goyal, D. F. Lee, M. Paranthaman, D. M. Kroeger, and D. K. Christen, Appl. Phys. Lett. **79**, 3998 (2001).
[3]A. Diaz, L. Mechin, P. Berghuis, and J. E. Evetts, Phys. Rev. B **58**, R2960 (1998).
[4]N. F. Heinig, R. D. Redwing, J. E. Nordman, and D. C. Larbalestier, Phys. Rev. B **60**, 1409 (1999).
[5]A. Gurevich, Annu. Rev. Condens. Matter Phys. **5**, 35 (2014).
[6]S. I. Kim, D. M. Feldmann, D. T. Verebelyi, C. Thieme, X. Le, A. A. Polyanskii, and D. C. Larbalestier, Phys. Rev. B **71**, 104501 (2005).
[7]D. M. Feldmann, T. G. Holesinger, R. Feenstra, and D. C. Larbalestier, J. Am. Ceram. Soc. **91**, 1869 (2008).
[8]M. F. Chisholm and S. J. Pennycook, Nature **351**, 47 (1991).
[9]S. E. Babcock and J. L. Vargas, Annu. Rev. Mater. Sci. **25**, 193 (1995).
[10]N. D. Browning, M. F. Chisholm, S. J. Pennycook, D. P. Norton, and D. H. Lowndes, Physica C **212**, 185 (1993).
[11]A. Schmehl, B. Goetz, R. R. Schulz, C. W. Schneider, H. Bielefeldt, H. Hilgenkamp, and J. Mannhart, Europhys. Lett. **47**, 110 (1999).
[12]G. Hammerl, A. Schmehl, R. R. Schulz, B. Goetz, H. Bielefeldt, C. W. Schneider, H. Hilgenkamp, and J. Mannhart, Nature **407**, 162 (2000).
[13]G. A. Daniels, A. Gurevich, and D. C. Larbalestier, Appl. Phys. Lett. **77**, 3251 (2000).
[14]M. A. Schofield, M. Beleggia, Y. Zhu, K. Guth, and C. Jooss, Phys. Rev. Lett. **92**, 195502 (2004).
[15]R. F. Klie, J. P. Buban, M. Varela, A. Franceschetti, C. Jooss, Y. Zhu, N. D. Browning, S. T. Pantelides, and S. J. Pennycook, Nature **435**, 475 (2005).
[16]X. Song, G. Daniels, D. M. Feldmann, A. Gurevich, and D. Larbalestier, Nat. Mater. **4**, 470 (2005).
[17]A. Gurevich and E. A. Pashitskii, Phys. Rev. B **57**, 13878 (1998).
[18]H. Su, D. O. Welch, and W. Wong-Ng, Phys. Rev. B **70**, 054517 (2004).
[19]J. Mannhart and H. Hilgenkamp, Mater. Sci. Eng. B **56**, 77 (1998).
[20]R. F. Klie, M. Beleggia, Y. Zhu, J. P. Buban, and N. D. Browning, Phys. Rev. B **68**, 214101 (2003).
[21]P. Li, D. Abraimov, A. Polyanskii, F. Kametani, and D. Larbalestier, Phys. Rev. B **91**, 104504 (2015).
[22]D. V. Abraimov, D. M. Feldmann, A. A. Polyanskii, A. Gurevich, S. Liao, G. Daniels, D. C. Larbalestier, A. P. Zhuravel, and A. V. Ustinov, IEEE Trans. Appl. Supercond. **15**, 2954 (2005).
[23]A. A. Polyanskii, A. Gurevich, A. E. Pashitskii, N. F. Heinig, R. D. Redwing, J. E. Nordman, and D. C. Larbalestier, Phys. Rev. B **53**, 8687 (1996).
[24]A. K. S. Kumar, T. Itoh, M. Kawasaki, and H. Koinuma, Physica C **349**, 83 (2001).
[25]E. F. Talantsev, N. M. Strickland, S. C. Wimbush, J. G. Storey, J. L. Tallon, and N. J. Long, Appl. Phys. Lett. **104**, 242601 (2014).
[26]A. Gurevich, M. S. Rzchowski, G. Daniels, S. Patnaik, B. M. Hinaus, F. Carillo, F. Tafuri, and D. C. Larbalestier, Phys. Rev. Lett. **88**, 097001 (2002).
[27]T. Haugan, P. N. Barnes, R. Wheeler, F. Meisenkothen, and M. Sumption, Nature **430**, 867 (2004).
[28]J. L. MacManus-Driscoll, S. R. Foltyn, Q. X. Jia, H. Wang, A. Serquis, L. Civale, B. Maiorov, M. E. Hawley, M. P. Maley, and D. E. Peterson, Nat. Mater. **3**, 439 (2004).

Published under license by AIP Publishing.